

Journal of
Mechanics of
Materials and Structures

**FINITE ELEMENT MODELING OF A LAYERED, MULTIPHASE
MAGNETOELECTROELASTIC CYLINDER SUBJECTED TO AN
AXISYMMETRIC TEMPERATURE DISTRIBUTION**

N. Ganesan, A. Kumaravel and Raju Sethuraman

Volume 2, N^o 4

April 2007



mathematical sciences publishers

FINITE ELEMENT MODELING OF A LAYERED, MULTIPHASE MAGNETOELECTROELASTIC CYLINDER SUBJECTED TO AN AXISYMMETRIC TEMPERATURE DISTRIBUTION

N. GANESAN, A. KUMARAVEL AND RAJU SETHURAMAN

This paper presents finite element formulation for dynamic behavior of magnetoelastoelectric axisymmetric cylinder coupled with a thermal field. The finite element formulation derived based on the interaction between mechanical, electrical, magnetic and thermal fields. The formulation is reduced to static case to analyze the static behavior of layered and multiphase magnetoelastoelectric axisymmetric cylinder under the circumstances of axisymmetric temperature distribution. The finite element model is developed using a four-noded axisymmetric element with four nodal degrees of freedom that is, two elastic displacements (u_r, u_z) with two potentials, electric (ϕ) and magnetic (ψ). The static behavior of axial and radial displacements, electric potential, magnetic potential and stresses on radially symmetric magnetoelastoelectric cylinder is investigated. The numerical results are compared between layered and multiphase magnetoelastoelectric cylinder with different boundary conditions.

1. Introduction

The combination of piezoelectric phase and piezomagnetic phase forms the layered and multiphase magnetoelastoelectric composites, which exhibit coupling effects between the mechanical/thermal, electrical and magnetic fields. It is also observed that the piezoelectric and piezomagnetic composites used for engineering structures, particularly in smart and intelligent structure systems in the recent years. Due to their ability of converting energy from one form to the other (among magnetic, electric and mechanical energies) these materials have been widely used in ultrasonic imaging devices, sensors, actuators, transducers and many other emerging components [Nan 1994; Harshe et al. 1993; Benveniste 1995; Ding et al. 2005]. There is a strong need for theories or techniques that can predict the coupled response of these smart materials, as well as structure composed of them. Various numerical studies have been carried out to study the behavior of composite laminates that consist of elastic and piezoelectric materials [Lee and Jian 1996; Heyliger 1997; Lee and Saravanas 1997, 2000; Vel and Batra 2000]. The generalized thermoelastic-piezoelectric coupled finite element equations are derived by Tianhu et al. [2002], based on the theory of Green–Lindsay with two relaxation times to solve the thermal shock problem. Buchanan [2003] has studied the behavior of infinitely long magnetoelastoelectric cylindrical shells using semianalytical finite element methods. Micro-mechanical analysis of fully coupled electromagnetothermoelastic composites has been carried out by Aboudi [2001] for prediction of the effective moduli of magnetoelastoelectric composites. Sunar et al. [2002] derived the finite element equations for thermopiezomagnetic medium based on linear constitutive equations using Hamilton’s principle. Wang and Zhong [2003] analytically

Keywords: layered and multiphase, axisymmetric temperature distribution, magnetoelastoelectric composites, dynamic behavior.

investigated a long cylindrical shell of piezoelectric/piezomagnetic composite under pressure loading and temperature change through the power series expansion method and the Fourier series expansion method. Surveying the literature, we found that there have been no studies are on magneto-electroelastic cylinder using finite element method under thermal environment. In this paper layered and multiphase magneto-electroelastic cylinder subjected to axisymmetric temperature distribution under different boundary conditions is investigated. Even though this paper presents the fully coupled finite element formulation, the numerical study is carried out for the thermal field decoupled with other fields.

2. Finite element formulation

The generalized governing differential equations for magneto-electrothermoelastic problem without body force, free charge, free current density or inner heat source can be written as

$$\sigma_{i,j} = \rho \ddot{u}_i, \quad D_{i,i} = 0, \quad B_{i,i} = 0, \quad q_{i,i} = -T_0 \rho \dot{\eta},$$

where ρ represents the mass density and T_0 represents the reference temperature. In a cylindrical coordinate system (r, θ, z) , the coupled constitutive equation for linearly magneto-electroelastic three-dimensional solid with thermal effect can be written as

$$\begin{aligned} \sigma_i &= c_{ij} S_j - e_{ik} E_k - d_{ik} H_k - \beta_{ij} \Theta, & D_l &= e_{lj} S_j + \varepsilon_{lk} E_k + m_{lk} H_k + p_l \Theta, \\ B_l &= d_{lj} S_j + m_{lk} E_k + \mu_{lk} H_k + \tau_l \Theta, & \rho \eta &= \beta_{ij} S_j + p_k E_k + \tau_k H_k + a \Theta, \end{aligned} \quad (1)$$

where $i, j = 1, \dots, 6$ and $l, k = 1, \dots, 3$. The reduced notation has been used for each tensor representations, ($\sigma_1 = \sigma_{rr}, \sigma_2 = \sigma_{\theta\theta}, \sigma_3 = \sigma_{zz}, \sigma_4 = \sigma_{\theta z}, \sigma_5 = \sigma_{rz}$ and $\sigma_6 = \sigma_{r\theta}$). σ_i, D_l, B_l, η are the components of stress, electric displacement, magnetic induction and entropy per unit volume; $c_{ij}, \varepsilon_{lk}, \mu_{lk}$ are the elastic, dielectric and magnetic permeability coefficients; e_{ki}, d_{ki}, m_{ik} are the piezoelectric, piezomagnetic and magneto-electric material coefficients; $\beta_{ij}, p_l, \tau_l, \Theta$ are stress temperature coefficient, pyroelectric constant, pyromagnetic constant and temperature difference; S_j, E_k, H_k are linear strain tensor, electric field and magnetic field vectors. $a = \rho C_E / T_0$, where C_E is the specific heat of the material. and $\Theta = T - T_0$ where T is absolute temperature and T_0 is reference temperature. The discretization of the finite element model is shown in [Figure 1](#).

The strain-displacement, electric field-electric potential and magnetic field-magnetic potential are used in the finite element analysis along with the constitutive [Equation \(1\)](#). The strain-displacement relation for axisymmetric case can be written as

$$S_{rr} = S_1 = \frac{\partial u_r}{\partial r}, \quad S_{\theta\theta} = S_2 = \frac{u_r}{r}, \quad S_{zz} = S_3 = \frac{\partial u_z}{\partial z}, \quad S_{zr} = S_5 = \frac{\partial u_z}{\partial r} + \frac{\partial u_r}{\partial z}.$$

The electric fields E_i , magnetic fields H_i and heat flux q_i are related to electric potential ϕ , magnetic potential ψ and temperature distribution Θ for axisymmetric case as

$$\begin{aligned} E_r &= E_1 = -\frac{\partial \phi}{\partial r}, & E_z &= E_3 = -\frac{\partial \phi}{\partial z}, & H_r &= H_1 = -\frac{\partial \psi}{\partial r}, & H_z &= H_3 = -\frac{\partial \psi}{\partial z}, \\ q_r &= q_1 = -k_{rr} \frac{\partial \Theta}{\partial r}, & q_z &= q_3 = -k_{zz} \frac{\partial \Theta}{\partial z}, \end{aligned}$$

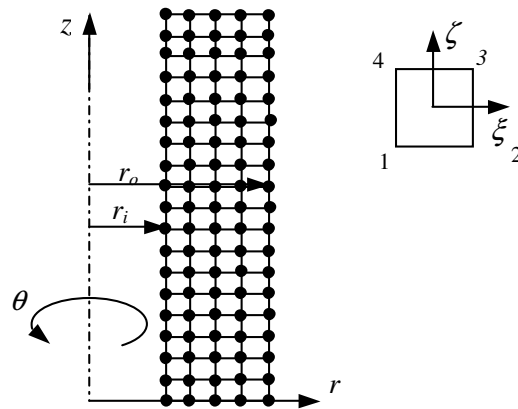


Figure 1. Schematic diagram of discretization of magnetoelectroelastic cylinder with four noded axisymmetric element.

where k is thermal conductivity of the material. For an axisymmetric cylinder geometry, load and material property does not vary in the circumferential direction. Semianalytical finite element approach for the axisymmetric problem, the displacements, electric potential and magnetic potential are expressed using Fourier series in the circumferential θ direction as

$$u_r = \sum u_r^n \cos n\theta, \quad u_\theta = \sum u_\theta^n \sin n\theta, \quad u_z = \sum u_z^n \cos n\theta, \quad \phi = \sum \phi^n \cos n\theta, \quad \psi = \sum \psi^n \cos n\theta,$$

where $n = 0$ for the axisymmetric problem. The analysis has been reduced for finite element in radial and axial direction. The finite element formulation of the coupled magnetoelctrothermoelastic problem is derived by approximating the displacement, electric potential, magnetic potential and temperature fields on the element level using two sets of shape functions:

$$\{u\} = [N_1^e]\{u^e\}, \quad \phi = [N_2^e]\{\phi^e\}, \quad \psi = [N_2^e]\{\psi^e\}, \quad \Theta = [N_2^e]\{\Theta^e\},$$

where $\{u^e\} = \{u_r \ u_\theta \ u_z\}^T$ is the displacement vector. For obtaining the element level governing equations, $\{S\}$, $\{E\}$ and $\{H\}$ are expressed in terms of derivatives of shape functions and elemental level degrees of freedom as,

$$\{S\} = [B_1]\{u^e\}, \quad \{E\} = -[B_2]\{\phi^e\}, \quad \{H\} = -[B_2]\{\psi^e\}, \quad \{\Theta'\} = [B_2]\{\Theta^e\},$$

where $[B]$ is the derivative of shape function matrix. It can be written as

$$[B_1] = \begin{bmatrix} \frac{\partial}{\partial r} & 0 \\ \frac{1}{r} & 0 \\ 0 & \frac{\partial}{\partial z} \\ \frac{\partial}{\partial z} & \frac{\partial}{\partial r} \end{bmatrix} \begin{bmatrix} N_1 & 0 & N_2 & 0 & N_3 & 0 & N_4 & 0 \\ 0 & N_1 & 0 & N_2 & 0 & N_3 & 0 & N_4 \end{bmatrix}, \quad [B_2] = \begin{bmatrix} -\frac{\partial}{\partial r} \\ -\frac{\partial}{\partial z} \end{bmatrix} [N_1 \ N_2 \ N_3 \ N_4].$$

Considering the body force $\{f\}$, the virtual displacement principle can be written as

$$\int_V (\delta\{S\}^T\{\sigma\} - \delta\{E\}^T\{D\} - \delta\{H\}^T\{B\} - \delta\Theta T_0\{\dot{\eta}\})dV = \int_V \delta\{u\}^T(\{f\} - \rho\{\ddot{u}\})dV + \int_{A_\sigma} \delta\{u\}^T\{\bar{t}\}dA + \int_{A_q} \delta\Theta\bar{q}dA, \quad (2)$$

where $\{\bar{t}\}$ represents the components of the traction vector and \bar{q} represents the heat flux. Substituting the constitutive relations from Equation (1) into Equation (2) and simplifying leads to

$$\int_V \delta\{S\}^T\{\sigma\}dV = \delta\{u^e\}^T \int_V [B_1]^T \left([c][B_1]\{u^e\} - [e](-[B_2]\{\phi^e\}) - [d](-[B_2]\{\psi^e\}) - \{\beta\}[N_2^e]^T\{\Theta^e\} \right) dV = \delta\{u^e\}^T \left([K_{uu}^e]\{u^e\} + [K_{u\phi}^e]\{\phi^e\} + [K_{u\psi}^e]\{\psi^e\} - [K_{u\Theta}^e]\{\Theta^e\} \right), \quad (3)$$

$$\int_V (-\delta\{E\}^T\{D\})dV = \delta\{\phi^e\}^T \int_V [B_2]^T \left([e]^T[B_1]\{u^e\} + [\varepsilon](-[B_2]\{\phi^e\}) + [m](-[B_2]\{\psi^e\}) + \{p\}[N_2^e]^T\{\Theta^e\} \right) dV = \delta\{\phi^e\}^T \left([K_{\phi u}^e]\{u^e\} - [K_{\phi\phi}^e]\{\phi^e\} - [K_{\phi\psi}^e]\{\psi^e\} + [K_{\phi\Theta}^e]\{\Theta^e\} \right), \quad (4)$$

$$\int_V (-\delta\{H\}^T\{B\})dV = \delta\{\psi^e\}^T \int_V [B_2]^T \left([d]^T[B_1]\{u^e\} + [m](-[B_2]\{\phi^e\}) + [\mu](-[B_2]\{\psi^e\}) + \{\tau\}[N_2^e]^T\{\Theta^e\} \right) dV = \delta\{\psi^e\}^T \left([K_{\psi u}^e]\{u^e\} - [K_{\psi\phi}^e]\{\phi^e\} - [K_{\psi\psi}^e]\{\psi^e\} + [K_{\psi\Theta}^e]\{\Theta^e\} \right), \quad (5)$$

$$\int_V (-\delta\Theta T_0\{\dot{\eta}\})dV = -\delta\{\Theta^e\}^T \int_V \left(T_0[N_2^e]\{\beta\}^T[B_1]\{\dot{u}^e\} + \{p\}^T(-[B_2]\{\dot{\phi}^e\}) + \{\tau\}^T(-[B_2]\{\dot{\psi}^e\}) + a[N_2^e]^T\{\dot{\Theta}^e\} \right) dV = \delta\{\Theta^e\}^T \left(-[C_{\Theta u}^e]\{\dot{u}^e\} + [C_{\Theta\phi}^e]\{\dot{\phi}^e\} + [C_{\Theta\psi}^e]\{\dot{\psi}^e\} - [C_{\Theta\Theta}^e]\{\dot{\Theta}^e\} \right), \quad (6)$$

$$\int_V \delta\{\Theta^e\}^T\{q\}dV = \delta\{\Theta^e\}^T \int_V [B_2]^T(-[k][B_2]\{\Theta^e\})dV = \delta\{\Theta^e\}^T(-[K_{\Theta\Theta}^e]\{\Theta^e\}), \quad (7)$$

$$\int_V \delta\{u\}^T(\{f\} - \rho\{\ddot{u}\})dV = \delta\{u^e\}^T \int_V [N_1^e]^T(\{f\} - \rho[N_1^e]\{\ddot{u}^e\})dV = \delta\{u^e\}^T(\{f_m^e\} - [M_{uu}^e]\{\ddot{u}^e\}), \quad (8)$$

$$\int_{A_\sigma} \delta\{u\}^T\{\bar{t}\}dA = \delta\{u^e\}^T \int_{A_\sigma} [N_1^e]\{\bar{t}\}dA = \delta\{u^e\}^T\{T_u^e\}, \quad (9)$$

$$\int_{A_q} \delta\Theta\{\bar{q}\}dA = \delta\{\Theta^e\}^T \int_{A_q} [N_2^e]\{\bar{q}\}dA = \delta\{\Theta^e\}^T\{T_\Theta^e\}. \quad (10)$$

From Equations (3)–(10) we can obtain

$$\begin{aligned}
 [M_{uu}^e]\{\ddot{u}^e\} - [C_{u\Theta}^e]\{\dot{\Theta}^e\} + [K_{uu}^e]\{u^e\} + [K_{u\phi}^e]\{\phi^e\} + [K_{u\psi}^e]\{\psi^e\} - [K_{u\Theta}^e]\{\Theta^e\} &= \{f_u^e\} + \{T_u^e\} \\
 [K_{u\phi}^e]^T\{u^e\} - [K_{\phi\phi}^e]\{\phi^e\} - [K_{\phi\psi}^e]\{\psi^e\} + [K_{\phi\Theta}^e]\{\Theta^e\} &= 0 \\
 [K_{u\psi}^e]^T\{u^e\} - [K_{\phi\psi}^e]^T\{\phi^e\} - [K_{\psi\psi}^e]\{\psi^e\} + [K_{\psi\Theta}^e]\{\Theta^e\} &= 0 \\
 [C_{\Theta u}^e]\{\dot{u}^e\} - [C_{\Theta\phi}^e]\{\dot{\phi}^e\} - [C_{\Theta\psi}^e]\{\dot{\psi}^e\} + [C_{\Theta\Theta}^e]\{\dot{\Theta}^e\} + [K_{\Theta\Theta}^e]\{\Theta^e\} &= -\{T_{\Theta}^e\}.
 \end{aligned}$$

Above equation can be expressed in the matrix form

$$\begin{aligned}
 \begin{bmatrix} M_{uu}^e & 0 & 0 & 0 \\ 0 & 0 & 0 & 0 \\ 0 & 0 & 0 & 0 \\ 0 & 0 & 0 & 0 \end{bmatrix} \begin{bmatrix} \ddot{u}^e \\ \ddot{\phi}^e \\ \ddot{\psi}^e \\ \ddot{\Theta}^e \end{bmatrix} + \begin{bmatrix} 0 & 0 & 0 & -C_{u\Theta}^e \\ 0 & 0 & 0 & 0 \\ 0 & 0 & 0 & 0 \\ C_{\Theta u}^e & -C_{\Theta\phi}^e & -C_{\Theta\psi}^e & C_{\Theta\Theta}^e \end{bmatrix} \begin{bmatrix} \dot{u}^e \\ \dot{\phi}^e \\ \dot{\psi}^e \\ \dot{\Theta}^e \end{bmatrix} + \\
 \begin{bmatrix} K_{uu}^e & K_{u\phi}^e & K_{u\psi}^e & -K_{u\Theta}^e \\ K_{\phi u}^e & -K_{\phi\phi}^e & -K_{\phi\psi}^e & K_{\phi\Theta}^e \\ K_{\psi u}^e & -K_{\psi\phi}^e & -K_{\psi\psi}^e & K_{\psi\Theta}^e \\ 0 & 0 & 0 & K_{\Theta\Theta}^e \end{bmatrix} \begin{bmatrix} u^e \\ \phi^e \\ \psi^e \\ \Theta^e \end{bmatrix} = \begin{bmatrix} f_u^e + T_u^e \\ 0 \\ 0 \\ -T_{\Theta}^e \end{bmatrix}, \quad (11)
 \end{aligned}$$

where different elemental matrices in Equation (11) are defined as

$$\begin{aligned}
 [K_{uu}^e] &= \int_V [B_1]^T [c] [B_1] dV, & [K_{u\phi}^e] &= \int_V [B_1]^T [e] [B_2] dV, \\
 [K_{u\psi}^e] &= \int_V [B_1]^T [d] [B_2] dV, & [K_{\phi\phi}^e] &= \int_V [B_2]^T [\varepsilon] [B_2] dV, \\
 [K_{\psi\psi}^e] &= \int_V [B_2]^T [\mu] [B_2] dV, & [C_{\Theta u}^e] &= \int_V T_0 [N_2]^T \{\beta\}^T [B_1] dV, \\
 [C_{\Theta\phi}^e] &= \int_V T_0 [N_2]^T \{p\}^T [B_2] dV, & [C_{\Theta\psi}^e] &= \int_V T_0 [N_2]^T \{\tau\}^T [B_2] dV, \\
 [K_{u\Theta}^e] &= \int_V [B_1]^T \{\beta\} [N_2]^T dV, & [K_{\phi\psi}^e] &= \int_V [B_2]^T [m] [B_2] dV, \\
 [K_{\phi\Theta}^e] &= \int_V [B_2]^T \{p\} [N_2]^T dV, & [K_{\psi\Theta}^e] &= \int_V [B_2]^T \{\tau\} [N_2]^T dV, \\
 [C_{\Theta\Theta}^e] &= \int_V T_0 [N_2]^T a [N_2] dV, & [K_{\Theta\Theta}^e] &= \int_V [B_2]^T [k] [B_2] dV, \\
 [M_{uu}^e] &= \int_V [N_1]^T \rho [N_1] dV, & \{f_u^e\} &= \int_V [N_1^e] \{f\} dV, \\
 \{T_u^e\} &= \int_{A_\sigma} [N_1^e]^T \{\bar{t}\} dA, & \{T_{\Theta}^e\} &= \int_{A_q} [N_2^e] \bar{q} dA.
 \end{aligned}$$

The volume integration is replaced with $dV = 2\pi r dr dz$ for axisymmetric problems. From Equation (11), assembling the all element contributions, the equation of motion can be written as,

$$[M]\{\ddot{v}\} + [D]\{\dot{v}\} + [K]\{v\} = \{F\}, \quad (12)$$

where

$$[M] = \begin{bmatrix} M_{uu} & 0 & 0 & 0 \\ 0 & 0 & 0 & 0 \\ 0 & 0 & 0 & 0 \\ 0 & 0 & 0 & 0 \end{bmatrix}, \quad [D] = \begin{bmatrix} 0 & 0 & 0 & -C_{u\Theta} \\ 0 & 0 & 0 & 0 \\ 0 & 0 & 0 & 0 \\ C_{\Theta u} & -C_{\Theta\phi} & -C_{\Theta\psi} & C_{\Theta\Theta} \end{bmatrix},$$

$$[K] = \begin{bmatrix} K_{uu} & K_{u\phi} & K_{u\psi} & -K_{u\Theta} \\ K_{\phi u} & -K_{\phi\phi} & -K_{\phi\psi} & K_{\phi\Theta} \\ K_{\psi u} & -K_{\psi\phi} & -K_{\psi\psi} & K_{\psi\Theta} \\ 0 & 0 & 0 & K_{\Theta\Theta} \end{bmatrix}, \quad \{F\} = \begin{bmatrix} f_u + T_u \\ 0 \\ 0 \\ -T_\Theta \end{bmatrix}, \quad \{v\} = \begin{bmatrix} u \\ \phi \\ \psi \\ \Theta \end{bmatrix},$$

with $\{u\} = [u_r \ u_z]^T$. The equation of motion (12) can be used to investigate the dynamic behavior of the magnetoelctrothermoelastic material where mechanical, electrical, magnetic and thermal fields are fully coupled. To investigate the static behavior of magnetoelctroelastic cylinder the above equation is reduced along with the following assumptions,

1. Absence of body force, free charge density and free current density.
2. The temperature distribution is evaluated explicitly assuming the coupling between mechanical, electrical and magnetic fields.

The finite element equation can be written as,

$$\begin{aligned} [K_{uu}]\{u\} + [K_{u\phi}]\{\phi\} + [K_{u\psi}]\{\psi\} &= \{F_{th}\}, \\ [K_{u\phi}]^T\{u\} - [K_{\phi\phi}]\{\phi\} - [K_{\phi\psi}]\{\psi\} &= 0, \\ [K_{u\psi}]^T\{u\} - [K_{\phi\psi}]^T\{\phi\} - [K_{\psi\psi}]\{\psi\} &= 0. \end{aligned} \quad (13)$$

The thermal load vector can be written as $\{F_{th}^e\} = \int_V [B_1]^T \{\beta\} \Theta dv$. By using standard condensation techniques, the equivalent stiffness matrix is derived by eliminating the electric potential ϕ and magnetic potential ψ in Equation (13). The derived stiffness matrix $[K_{eq}]$ and load vector $\{F_{th}\}$ is used to solve for nodal thermal displacements.

$$[K_{eq}]\{u\} = \{F_{th}\}, \quad (14)$$

where $[K_{eq}] = [K_{uu}] + [K_{u\phi}][K_{II}]^{-1}[K_I] + [K_{u\psi}][K_{IV}]^{-1}[K_{III}]$, and

$$\begin{aligned} [K_I] &= [K_{u\phi}]^T - [K_{\phi\psi}][K_{\psi\psi}]^{-1}[K_{u\psi}]^T, & [K_{II}] &= [K_{\phi\phi}] - [K_{\phi\psi}][K_{\psi\psi}]^{-1}[K_{\phi\psi}]^T, \\ [K_{III}] &= [K_{u\psi}]^T - [K_{\phi\psi}]^T[K_{\phi\phi}]^{-1}[K_{u\phi}]^T, & [K_{IV}] &= [K_{\psi\psi}] - [K_{\phi\psi}]^T[K_{\phi\phi}]^{-1}[K_{\phi\psi}]. \end{aligned}$$

The coupled magnetoelctroelastic finite element Equation (14) is solved subject to thermal loading. The four-point gaussian integration scheme has been adopted to evaluate the integrals involved in different elemental stiffness matrices and thermal load vectors. The elemental stiffness matrices and thermal load vectors are assembled to get the global stiffness matrices and global thermal load vector. The coupled equivalent stiffness matrix $[K_{eq}]$ of magnetoelctroelastic system has been inverted to evaluate the thermal displacements. After evaluating the thermal displacements, the electric potential ϕ and magnetic potential ψ can be derived at each nodal points using the following equations,

$$\phi = [K_{II}]^{-1}[K_I]\{u\}, \quad \psi = [K_{IV}]^{-1}[K_{III}]\{u\}.$$

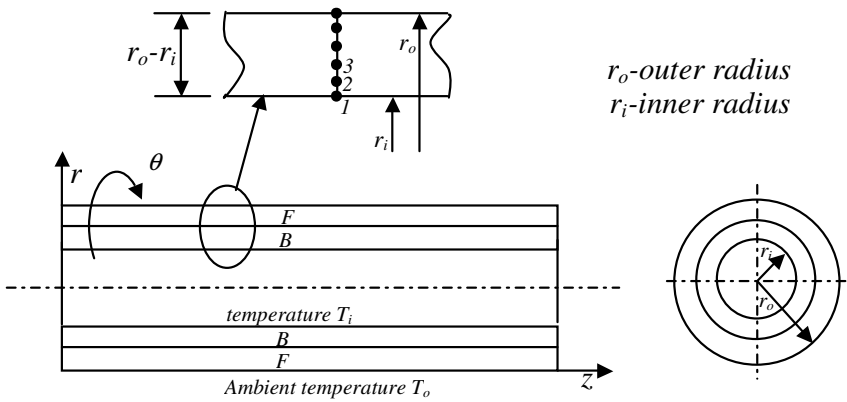


Figure 2. Schematic diagram of layered magneto-electro-elastic hollow cylinder along with thermal boundary conditions.

3. Evaluation of temperature distribution across the thickness of the axisymmetric cylinder under steady state heat conduction

We consider steady state one-dimensional heat conduction analysis to evaluate the temperature distribution across the thickness of the magneto-electro-elastic cylinder under temperature boundary conditions. The temperature along the length of the cylinder is constant subject to axisymmetric temperature distribution. Figure 2 shows the schematic diagram of problem considered for steady state heat conduction analysis and finite element discretization across thickness direction. The finite element formulation used in the present work is based on the procedure reported in [Reddy 1984]. By neglecting the convective and radiation heat transfers, the governing differential equation for steady state heat conduction equation in radial direction is given by

$$-\frac{d}{dr} \left(k(r) \frac{dT}{dr} \right) = 0.$$

In the present study, thermal boundary conditions considered in such a way that T_i is the temperature on the inner surface of the cylinder and T_0 is the temperature on the outer surface of the cylinder, which is normally ambient temperature. Applying variational principle on the governing equation, the finite element equation $[K_{cond}]\{T\} = 0$, to evaluate temperature distribution due to heat conduction is obtained [Ross 1990]. Here $[K_{cond}]$ is the heat conduction matrix and $\{T\}$ is the vector of nodal temperature.

The above equation is solved for the specified temperature boundary condition at the inner and outer surface to obtain the temperature distribution across the radial direction.

4. Validation of the present formulation

The present formulation developed for the analysis of layered and multiphase magneto-electro-elastic cylinder has been validated with the stresses reported in [Wang and Zhong 2003] under internal pressure loading.

The dimensions of cylinder are as follows: length of the cylinder (l) = 4.0 m, inner radius (r_i) = 0.7 m and thickness of the cylinder (t) = 0.6 m. Figure 3 illustrates the comparison of results of axial

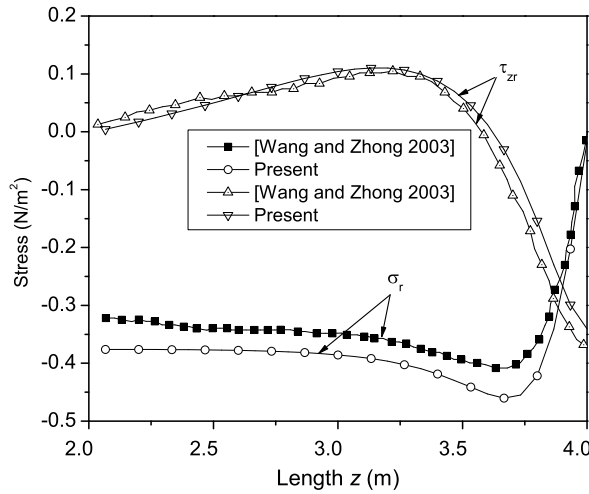


Figure 3. Variation of normal radial stress σ_r and shear stress τ_{zr} on the outer surface at $r = r_o$ along the axial direction subjected to internal pressure loading under simply supported boundary condition.

stresses for B/F layered magneto-electroelastic cylinder under internal pressuring loading with simply supported boundary condition. The thermal load vector have been validated using commercial finite element software [ANSYS 1999], by evaluating the thermal displacement along the axial length of simply supported piezoelectric cylinder under uniform temperature rise of 75°C .

Figure 4 illustrates the comparison of results on thermal displacement for simply supported piezoelectric cylinder. This was performed primarily because of the lack of literature on the evaluation of thermal

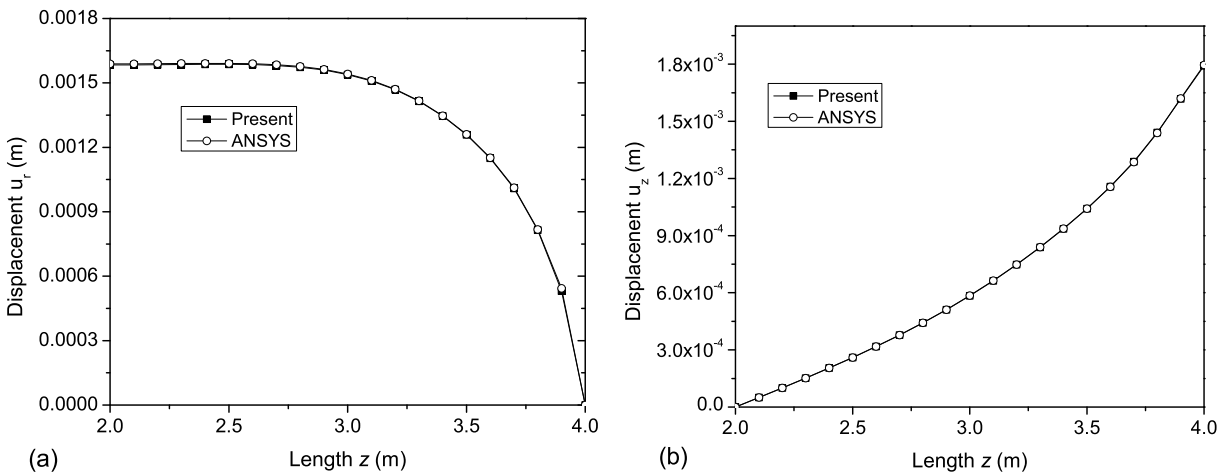


Figure 4. Variation (a) radial displacement u_r and (b) axial displacement u_z on the outer surface at $r = r_o$ subjected to uniform temperature rise.

stresses of magneto-electroelastic cylinder using finite element method. Observe that the results obtained by present formulation are in close agreement with the available literature and commercial finite element software ANSYS.

5. Results and discussions

We consider a two layered and multiphase magneto-electroelastic composite cylinder composed of piezo-electric BaTiO₃ and piezomagnetic CoFe₂O₄ materials. Two-layered cylinder is made of the inner surface with piezoelectric BaTiO₃ material and outer surface made of piezomagnetic CoFe₂O₄ material (B/F). The multiphase magneto-electroelastic cylinder made of piezomagnetic (CoFe₂O₄) matrix reinforced by piezoelectric (BaTiO₃) material for different volume fraction. The $V_f = 1.0$ corresponds to piezoelectric (BaTiO₃) material and $V_f = 0.0$ corresponds to piezomagnetic (CoFe₂O₄) material. The dimensions of cylinder are as follows: length of the cylinder (l) = 4.0 m, inner radius (r_i) = 0.995 m, thickness of the cylinder (t) = 0.01 m, r/t ratio = 100, l/r ratio = 4.0. The present finite element model is discretized using 600 four-noded axisymmetric elements with 3355 degrees of freedom (dof): 2013 displacement dof, 671 electric dof and 671 magnetic dof. The simply supported and clamped-clamped ($u_r = \phi = \psi = 0$ at simply supported edge and $u_r = u_z = \phi = \psi = 0$ at clamped edge) boundary conditions are adopted. The material constants listed in Table 1 reported by Aboudi [2001] are used for the present study. The thermal conductivity k and the coefficient of thermal expansion α are obtained from the literature as reported by Ootao and Tanigawa [2005]. In the above literature the coefficient of thermal expansion α is taken for CoFe₂O₄. The diffusivities for BaTiO₃ and CoFe₂O₄ given in [Ootao and Tanigawa 2005] are not needed, since the present analysis assumed as steady state problem. Thermal properties are not reported in the literature for different volume fraction. The coefficient of thermal expansion are evaluated from the values of BaTiO₃ and CoFe₂O₄ for different volume fractions of 0.2, 0.4, 0.6 and 0.8 using the following expression [Tan and Tong 2002]:

$$\alpha_{11} = c_{11} \left(\frac{V_f \alpha_{11}^p}{c_{11}^p} + \frac{(1 - V_f) \alpha_{11}^m}{c_{11}^m} \right), \quad \alpha_{33} = V_f \alpha_{33}^p + (1 - V_f) \alpha_{33}^m + \frac{c_{13} \alpha_{11}}{c_{11}} - \frac{V_f c_{13}^p \alpha_{11}^p}{c_{11}^p} - \frac{(1 - V_f) c_{13}^m \alpha_{11}^m}{c_{11}^m}.$$

The densities reported by Ramirez et al. [2006] for BaTiO₃ and CoFe₂O₄ are used for the present analysis. The density and thermal conductivities are evaluated from the values of BaTiO₃ and CoFe₂O₄ using the rule of mixture,

$$\rho = V_f \rho^p + (1 - V_f) \rho^m, \quad k_{11} = k_{33} = V_f k_{11}^p + (1 - V_f) k_{11}^m,$$

where the superscript p stands for piezoelectric and m stands for piezomagnetic.

Evaluation of temperature distribution. The magneto-electroelastic cylinder is discretized using two-noded element with temperature degree of freedom as shown in Figure 2. These nodal temperatures are used to evaluate the element temperature of four-noded axisymmetric element and utilized to evaluate thermal load vector. Figure 5 shows the temperature distribution across thickness direction for layered and multiphase magneto-electroelastic cylinder.

Distribution of displacement, electric potential, magnetic potential and thermal stresses subjected to simply supported boundary condition. Figure 6(a) shows the distribution of radial displacement u_r on

	$V_f = 0.0$	$V_f = 0.2$	$V_f = 0.4$	$V_f = 0.6$	$V_f = 0.8$	$V_f = 1.0$
<i>Elastic constants</i>						
c_{11}	269.5	240	220	190	170	162
$c_{12} = c_{13}$	170	145	125	110	100	78
c_{23}	173	146	125	110	100	77
$c_{22} = c_{33}$	286	250	225	200	175	166
c_{55}	45.3	45	45	45	50	43
<i>Piezoelectric constants</i>						
e_{11}	0	4	7	11	14	18.6
$e_{12} = e_{13}$	0	-2	-3	-3.5	-4	-4.4
e_{35}	0	0	0	0	0	11.6
<i>Dielectric constants</i>						
ϵ_{11}	0.093	2.5	5.0	7.5	10	12.6
ϵ_{33}	0.08	0.33	0.8	0.9	1.0	11.2
<i>Magnetic permeability constants</i>						
μ_{11}	1.57	1.33	1.0	0.75	0.5	0.1
μ_{33}	-5.9	-3.9	-2.5	-1.5	-0.8	0.05
<i>Piezomagnetic constants</i>						
q_{11}	700	550	380	260	120	0
$q_{12} = q_{13}$	580	410	300	200	100	0
q_{35}	560	340	220	180	80	0
<i>Magnetolectric constants</i>						
m_{11}	0	2000	2750	2500	1500	0
m_{33}	0	2.8	4.8	6.0	6.8	0
<i>Coefficient of thermal expansion</i>						
α_{11}	10.0	9.72	9.15	8.37	7.44	6.4
α_{33}	10.0	11.7	13.0	14.11	14.98	15.7
<i>Density</i>						
ρ	5300	5400	5500	5600	5700	5800
<i>Thermal conductivity</i>						
$k_{11} = k_{33}$	3.2	3.06	2.92	2.78	2.64	2.5

Table 1. Material properties as a percentage (volume fraction V_f) of $\text{CoFe}_2\text{O}_4 - \text{BaTiO}_3$, where c_{ij} is measured in 10^9 N/m^2 , e_{ij} in C/m^2 , ϵ_{ij} in 10^{-9} C/Vm , q_{ij} in N/Am , μ_{ij} in $10^{-4} \text{ N s}^2/\text{C}^2$, m_{ij} in 10^{-12} N s/VC , α_{ij} in $1/\text{K}$, ρ in kg/m^3 , and k_{ij} in W/mK .

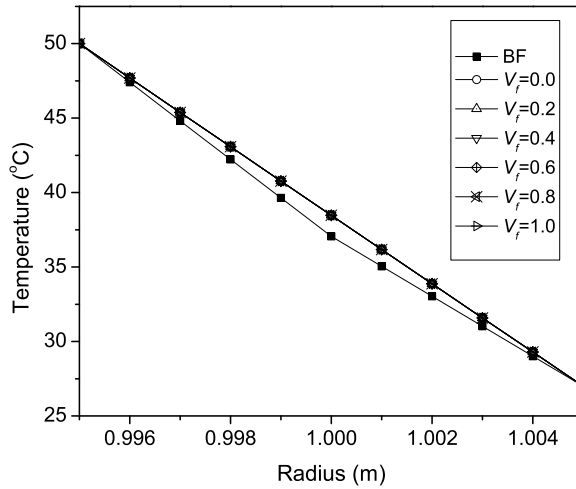


Figure 5. Distribution of temperature across thickness direction for layered and multi-phase magnetoelastoelectroelastic cylinder.

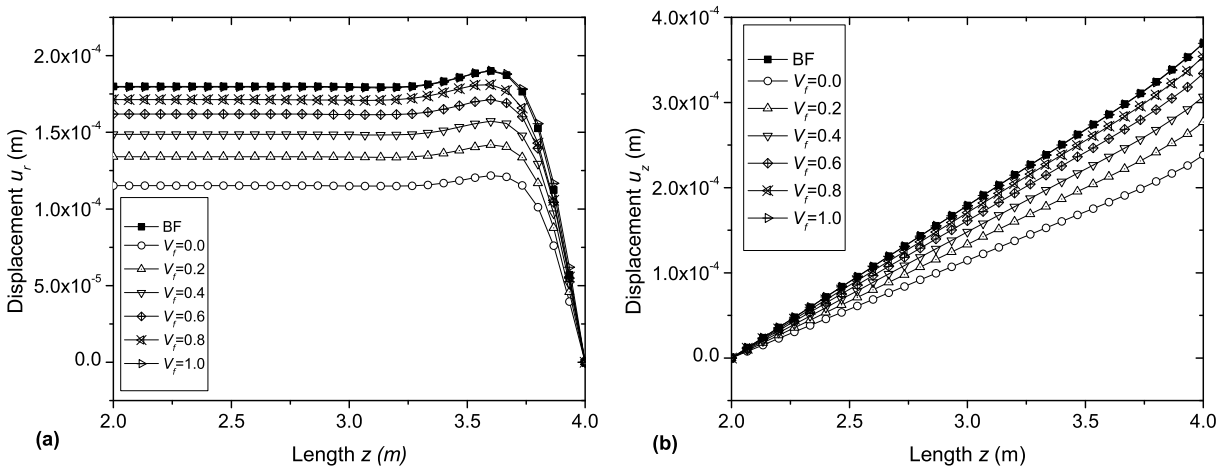


Figure 6. Distribution of (a) radial displacement u_r and (b) axial displacement u_z on the outer surface at $r = r_o$ along the axial direction under simply-supported boundary condition.

the outer surface along the axial direction for B/F layered and multiphase with different volume fraction of magnetoelastoelectroelastic cylinder. It is observed that the radial displacement u_r of B/F layered cylinder is slightly higher as compared to multiphase magnetoelastoelectroelastic cylinder with $V_f = 1.0$. The radial displacement is increasing with volume fraction of multiphase magnetoelastoelectroelastic cylinder and the magnitude is higher near the simply supported edge. Figure 6(b) shows the axial displacement u_z on the outer surface along the axial direction. Observe that the magnitude of axial displacement u_z is higher at

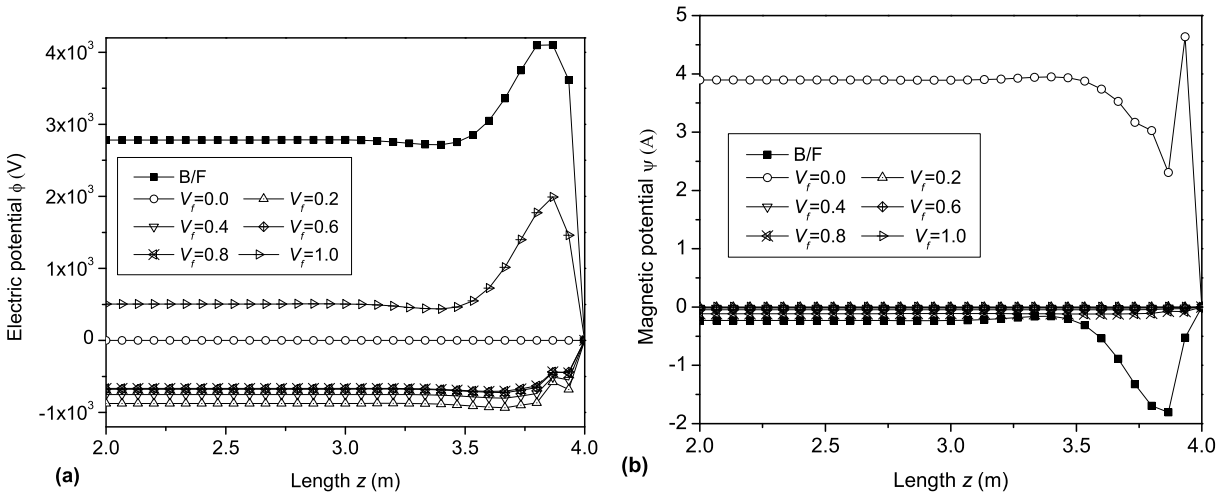


Figure 7. Distribution of (a) electric potential ϕ and (b) magnetic potential ψ on the outer surface at $r = r_o$ along the axial direction under simply-supported boundary condition.

the simply supported edge. The axial displacement u_z is increasing with volume fraction of multiphase magneto-electroelastic cylinder.

Figure 7(a) shows the distribution of electric potential ϕ on the outer surface along the axial direction for B/F layered and multiphase with different volume fraction of magneto-electroelastic cylinder. It is observed that the electric potential is higher for B/F layered case as compared to multiphase magneto-electroelastic cylinder and magnitude is higher near the simply supported edge. Figure 7(b) shows the distribution of magnetic potential ψ on the outer face along the axial direction.

The magnetic potential is higher for $V_f = 0.0$ as compared to other volume fraction and B/F layered cylinder. Figure 8(a) shows the distribution of radial displacement u_r at $z = l/2$ along the radial direction for B/F layered and multiphase with different volume fraction of magneto-electroelastic cylinder. Observe that the B/F layered radial displacement u_r is higher as compared to multiphase magneto-electroelastic cylinder. It is increases with volume fraction for multiphase case. Figure 8(b) shows the distribution of axial displacement u_z at $z = l$ along the radial direction for B/F layered and multiphase magneto-electroelastic cylinder. Note that the similar trend is observed for axial displacement u_z .

Figure 9 illustrates the distribution of electric potential ϕ and magnetic potential ψ at $z = l/2$ along the radial direction for B/F layered and multiphase multiphase magneto-electroelastic cylinder. Observe that the electric potential ϕ is higher for layered magneto-electroelastic case and magnetic potential ψ is higher for $V_f = 0.0$. Note that variation of electric potential ϕ in the piezoelectric phase and constant in the piezomagnetic phase. The electric potential ϕ is zero for $V_f = 0.0$ due to the fact that the piezoelectric constants are zero. Figure 9(b) illustrates the variation of magnetic potential ψ at $z = l/2$ along the radial direction for B/F layered and multiphase magneto-electroelastic cylinder.

Figure 10 illustrates the distribution of normal stress σ_r and shear stress τ_{zr} at $r = 0.005$ m along the axial direction for B/F layered and multiphase magneto-electroelastic cylinder. Observe that the normal

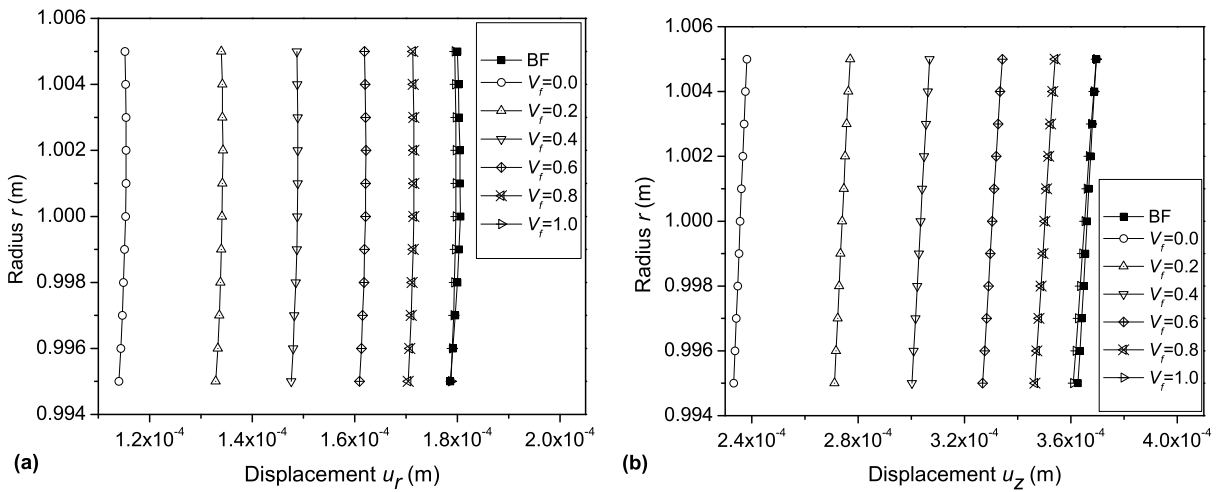


Figure 8. Distribution of (a) radial displacement u_r at $z = l/2$ and (b) axial displacement u_z at $z = l$ along the radial direction under simply-supported boundary condition.

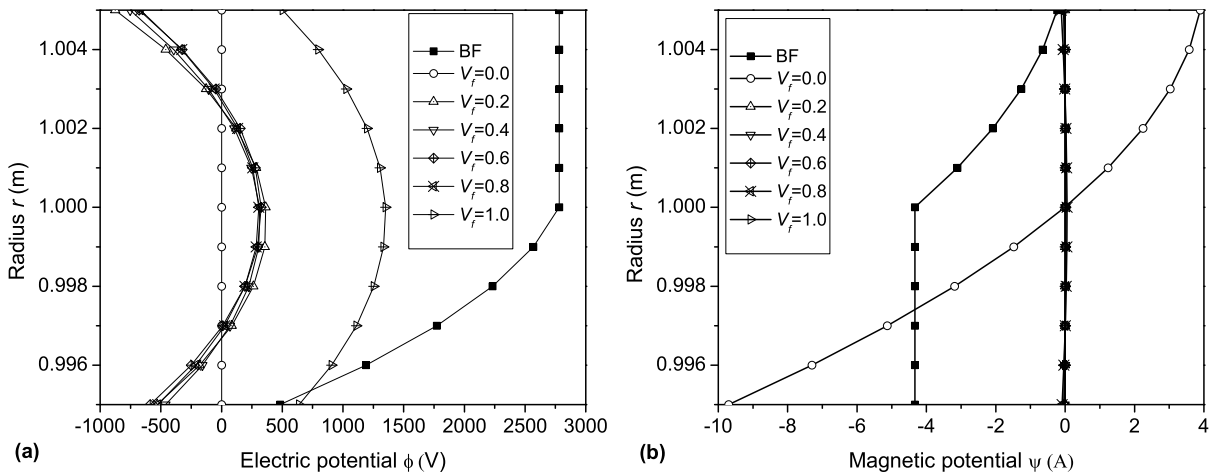


Figure 9. Distribution of (a) electric potential ϕ and (b) magnetic potential ψ at $z = l/2$ along the radial direction under simply-supported boundary condition.

stress σ_r for layered cylinder is higher as compared to multiphase cylinder and there is no significant effect on shear stress τ_{zr} . [Figure 11](#) illustrates the distribution of normal stress σ_r and σ_θ for B/F layered magneto-electroelastic cylinder at $z = l/2$ along the radial direction.

Note the discontinuity of radial stress σ_r at the material interface. Observe that the normal stress σ_θ compressive in nature at the inner surface and tensile on the outer surface. [Figure 12](#) shows the distribution of normal stress σ_r and σ_θ at $z = l/2$ along the radial direction. It is noticed that the normal stress σ_r increases with volume fraction decreases for multiphase magneto-electroelastic cylinder. It can

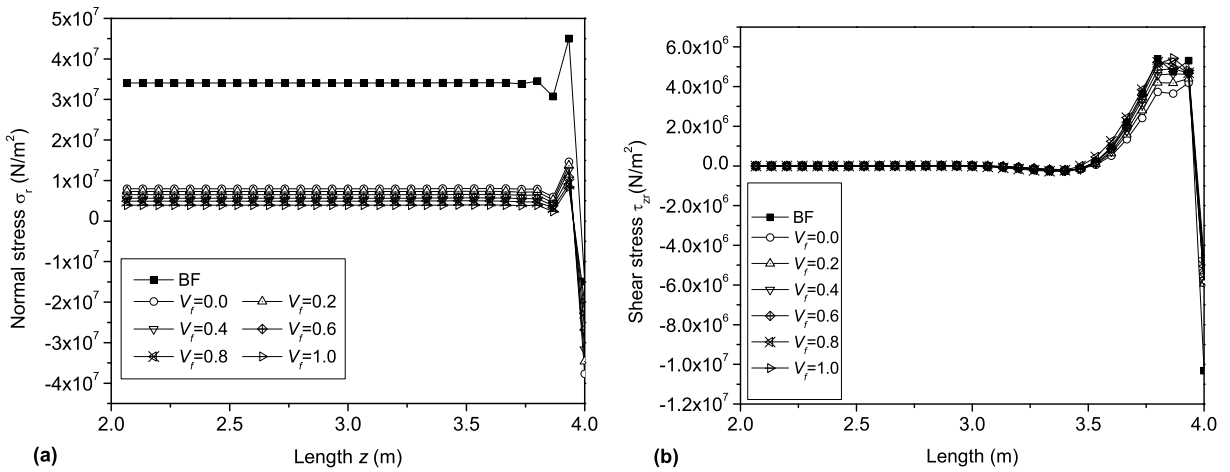


Figure 10. Distribution of (a) normal stress σ_r and (b) shear stress τ_{zr} at $r = 0.005$ m along the axial direction under simply-supported boundary condition.

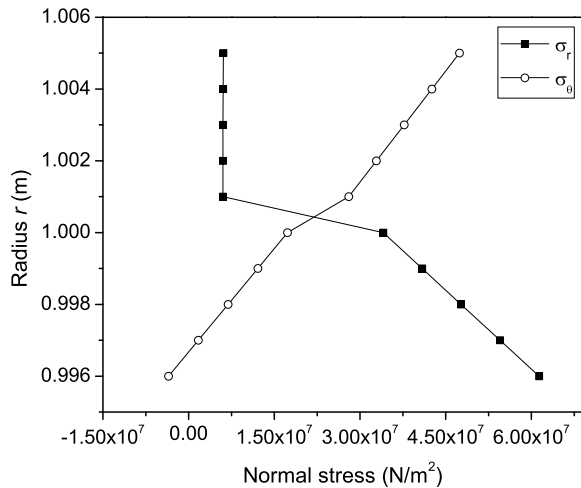


Figure 11. Distribution of normal stress σ_r and σ_θ for B/F layered magneto-electro-elastic cylinder at $z = l/2$ along the radial direction under simply-supported boundary condition.

be seen that the normal stress σ_θ compressive in nature at the inner surface and tensile on the outer surface. Its magnitude is minimum for $V_f = 0.0$ and maximum for $V_f = 1.0$.

Distribution of displacement, electric potential, magnetic potential and thermal stresses subjected to clamped-clamped boundary condition. Figure 13(a) shows the distribution of radial displacement u_r on the outer surface along the axial direction for B/F layered and multiphase with different volume fraction of magneto-electro-elastic cylinder under clamped-clamped boundary condition.

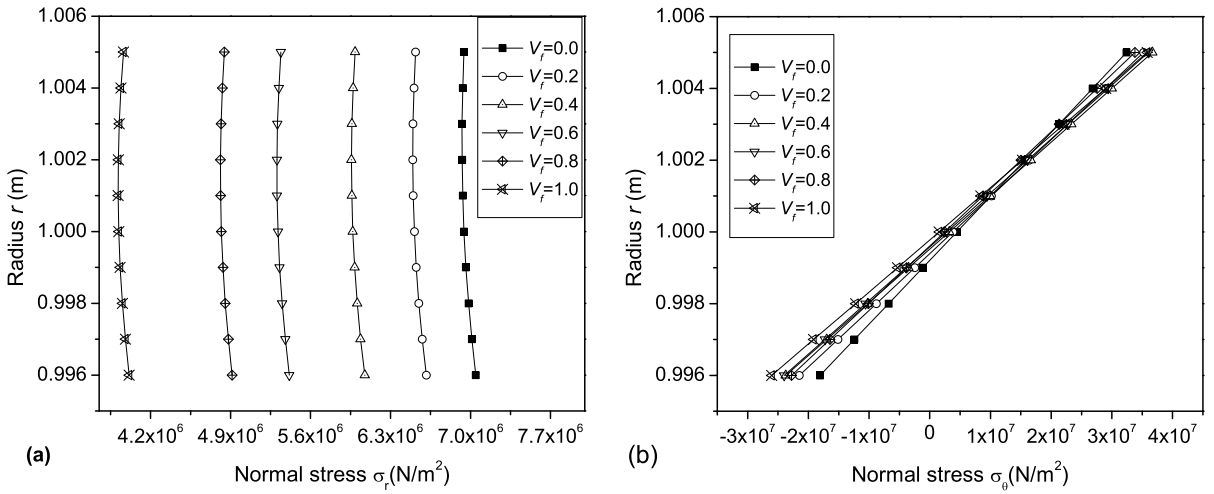


Figure 12. Distribution of (a) normal stress σ_r and (b) normal stress σ_θ at $z = l/2$ along the radial direction under simply-supported boundary condition.

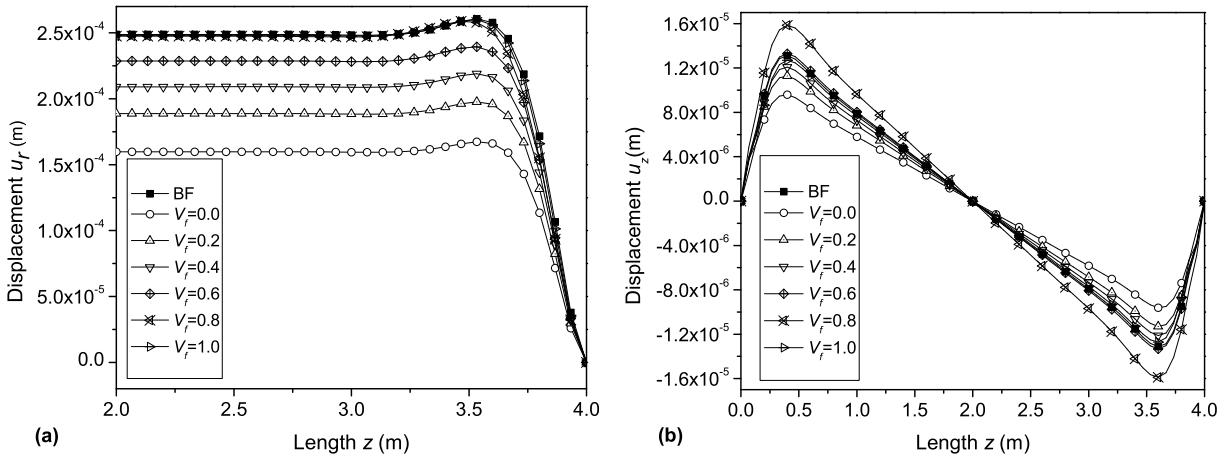


Figure 13. Distribution of (a) radial displacement u_r ($l = 2.0$ to 4.0 m) and (b) axial displacement u_z ($l = 0.0$ to 4.0 m) on the outer surface at $r = r_o$ along the axial direction under clamped-clamped boundary condition.

A similar trend is observed compared to simply supported boundary condition with higher radial displacement. From [Figure 13\(b\)](#), it is observed that the maximum axial displacement occurs near the clamped edge and the distribution is quite different as compared to simply supported boundary condition. [Figure 14\(a\)](#) shows the distribution of electric potential ϕ on the outer surface along the axial direction for clamped-clamped boundary condition. The maximum electric potential occurs close to the clamped edge, further the electric potential decreases and remains constant in magnitude over the length of the cylinder. The zero electric potential for $V_f = 0.0$ due to fact that the piezoelectric constants are zero.

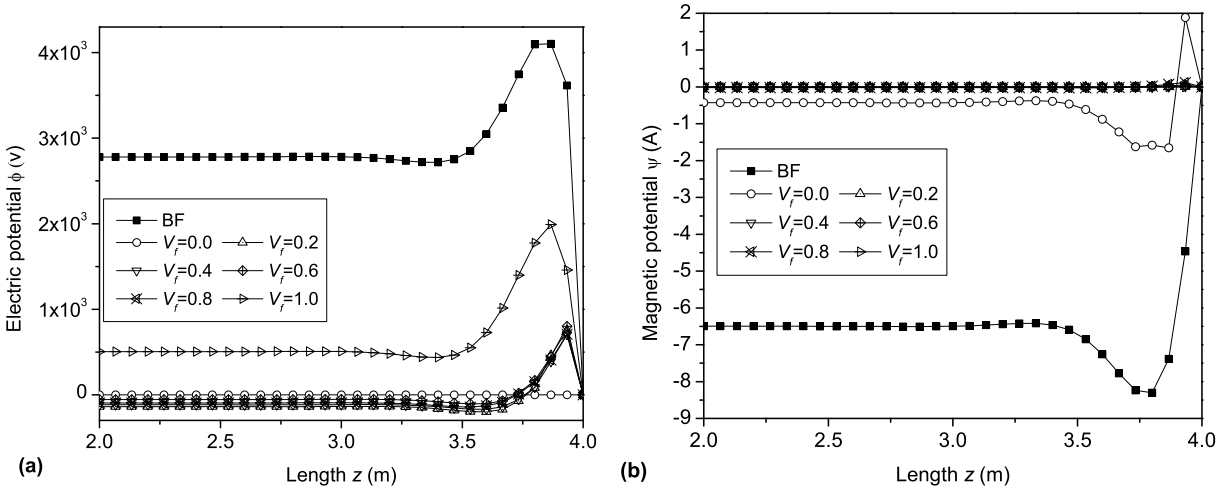


Figure 14. Variation of (a) electric potential ϕ and (b) magnetic potential ψ on the outer surface at $r = r_o$ along the axial direction under clamped-clamped boundary condition.

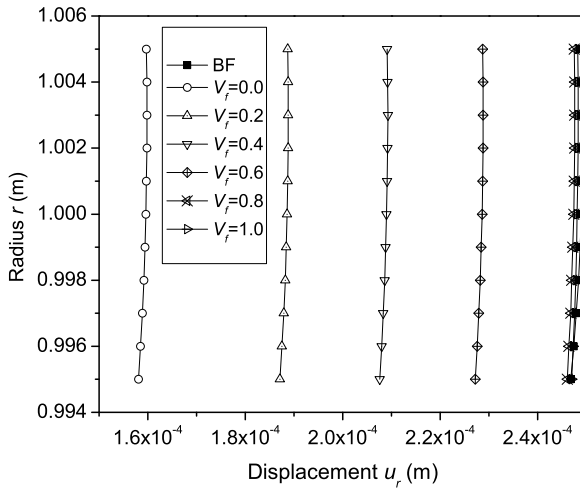


Figure 15. Distribution of radial displacement u_r at $z = l/2$ along the radial direction subjected to thermal loading under clamped-clamped boundary condition.

Figure 14(b) shows the distribution of magnetic potential ψ on the outer surface along the axial direction for clamped-clamped boundary condition.

Figure 15 shows the distribution of radial displacement u_r at $z = l/2$ along the radial direction subjected to thermal loading under clamped-clamped boundary condition. Observe that the radial displacement u_r is higher as compared to simply supported boundary condition and increasing with volume fraction. This is because the stiffness is greater for $V_f = 0.0$ and less for $V_f = 1.0$ due to elastic properties of materials.

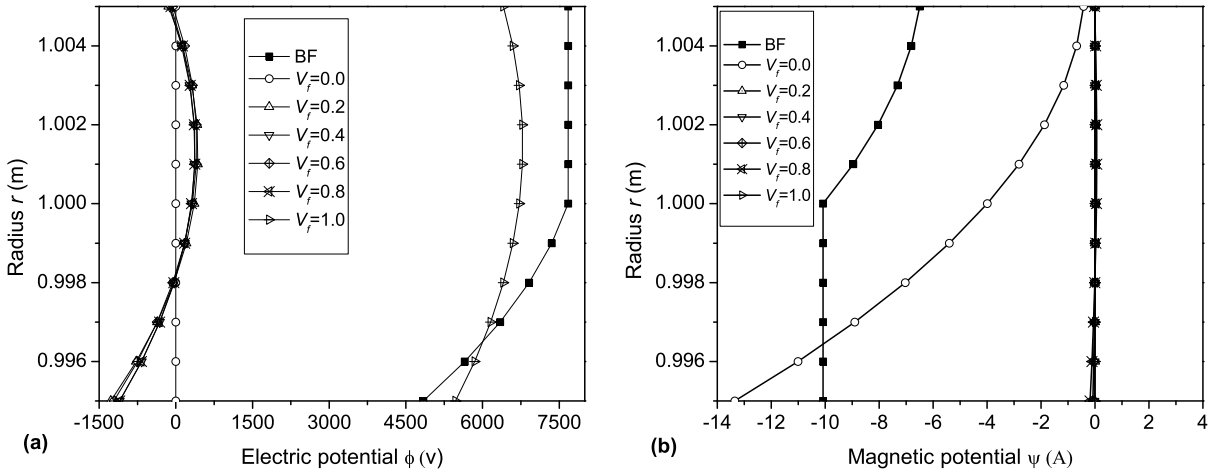


Figure 16. Distribution of (a) electric potential ϕ and (b) magnetic potential ψ at $z = l/2$ along the radial direction subjected to thermal loading under clamped-clamped boundary condition.

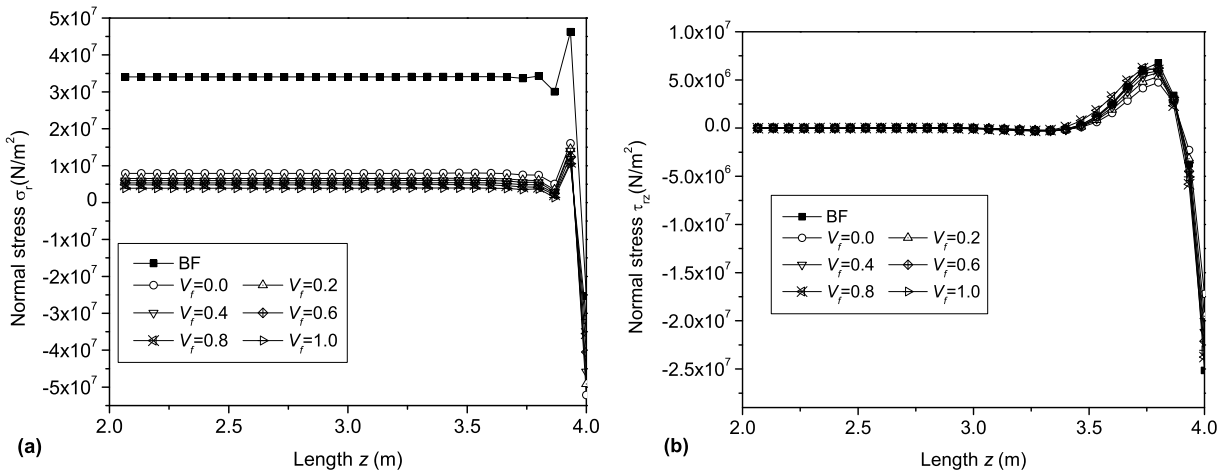


Figure 17. Distribution of (a) normal stress σ_r and (b) shear stress τ_{zr} at $r = 0.005$ m along the axial direction under clamped-clamped boundary condition.

Figure 16 illustrates the distribution of electric potential ϕ and magnetic potential ψ at $z = l/2$ along the radial direction for clamped-clamped magneto-electroelastic cylinder. A similar trend is observed with higher magnitude compared to simply supported boundary condition. Figure 17 illustrates the distribution of normal stress σ_r and shear stress τ_{zr} at $r = 0.005$ m along the axial direction for clamped-clamped magneto-electroelastic cylinder. Observe that the normal stress σ_r is higher for B/F layered cylinder.

There is no significant difference along the length and higher in the clamped end as compared to Simply-Supported boundary condition. Figures 18 and 19 illustrate the distribution of normal stress σ_r ,

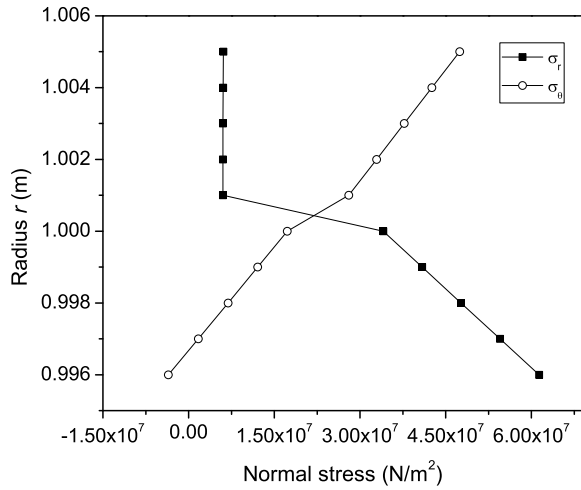


Figure 18. Distribution of normal stress σ_r and σ_θ for B/F layered magneto-electroelastic shell at $z = l/2$ along the radial direction under clamped-clamped boundary condition.

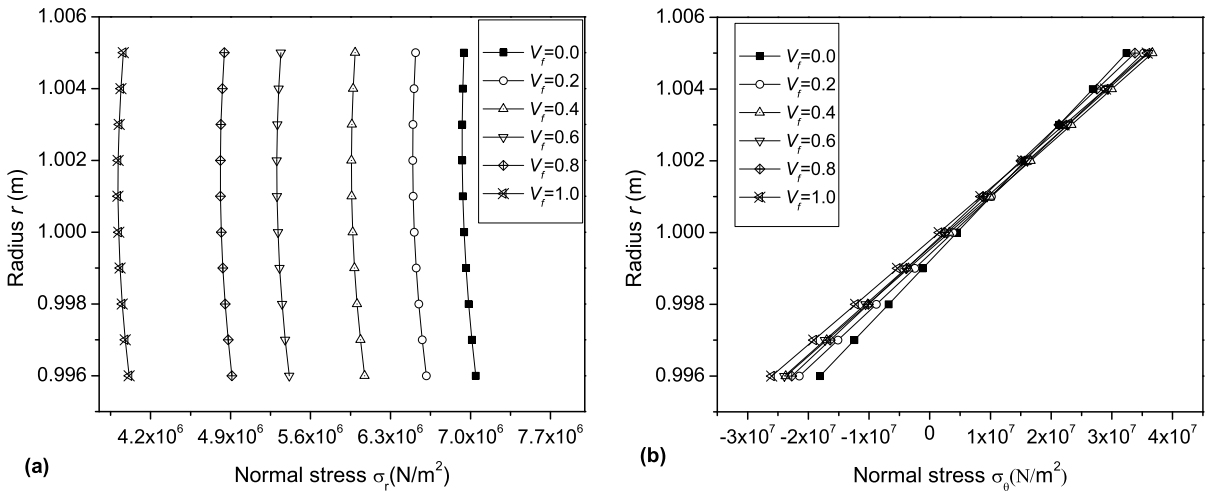


Figure 19. Distribution of (a) normal stress σ_r and (b) normal stress σ_θ at $z = l/2$ along the radial direction subjected to thermal loading under clamped-clamped boundary condition.

and σ_θ for B/F layered magneto-electroelastic cylinder at $z = l/2$ along the radial direction and normal stress σ_r and σ_θ for multiphase magneto-electroelastic cylinder at $z = l/2$ along the radial direction. A similar behavior is observed compared to afore mentioned boundary condition.

6. Conclusions

A semi-analytical finite element model is used for the analysis of layered and multiphase magneto-electro-elastic cylinder under axisymmetric temperature distribution. The finite element formulation for transient analysis of magneto-electrothermoelastic cylinder has been derived from coupled constitutive equations. The numerical results are presented based on the coupling between mechanical, electrical and magnetic fields. The thermal field is coupled with mechanical fields alone. It is found that the layered magneto-electroelastic cylinder have substantial effect on induced magnetic, electric and elastic fields as compared to multiphase magneto-electroelastic cylinder with different volume fraction under different boundary conditions. We feel that the present numerical study is highly useful for design of magneto-electroelastic sensors and actuators.

References

- [Aboudi 2001] J. Aboudi, "Micromechanical analysis of fully coupled electro-magneto-thermo-elastic multiphase composites", *Smart Mater. Struct.* **10** (2001), 867–877.
- [ANSYS 1999] ANSYS Inc., *ANSYS theory manual, Structural analysis guide*, ANSYS Inc., 1999.
- [Benveniste 1995] Y. Benveniste, "Magneto-electric effect in fibrous composites with piezoelectric and piezomagnetic phases", *Phys. Rev. B* **51** (1995), 16424–16427.
- [Buchanan 2003] B. R. Buchanan, "Free vibration of an infinite magneto-electro-elastic cylinder", *J. Sound Vib.* **268** (2003), 413–426.
- [Ding et al. 2005] H. Ding, A. Jiang, P. Hou, and W. Chen, "Green's functions for two-phase transversely isotropic magneto-electro-elastic media", *Eng. Anal. Bound. Elem.* **29** (2005), 551–561.
- [Harshe et al. 1993] G. Harshe, J. P. Dougherty, and R. E. Mewham, "Theoretical modeling of multilayer magneto-electric composites", *Int. J. Appl. Electromagn. Mater.* **4** (1993), 145–159.
- [Heyliger 1997] P. Heyliger, "Exact solutions for simply supported laminated piezoelectric plates", *J. Appl. Mech.* **64** (1997), 299–306.
- [Lee and Jian 1996] J. S. Lee and L. Z. Jian, "Exact electroelastic analysis of piezoelectric laminae via state space approach", *Int. J. Solids Struct.* **33** (1996), 977–990.
- [Lee and Saravanos 1997] H. J. Lee and D. A. Saravanos, "Generalized finite element formulation for smart multilayered thermal piezoelectric composite plates", *Int. J. Solids Struct.* **34** (1997), 3355–3371.
- [Lee and Saravanos 2000] H. J. Lee and D. A. Saravanos, "A mixed multi-field finite element formulation for thermopiezoelectric composite shells", *Int. J. Solids Struct.* **37** (2000), 4949–4967.
- [Nan 1994] C. W. Nan, "Magneto-electric effect in composites of piezoelectric and piezomagnetic phases", *Phys. Rev. B* **50** (1994), 6082–6088.
- [Ootao and Tanigawa 2005] Y. Ootao and Y. Tanigawa, "Transient analysis of multilayered and magneto-electro-thermo elastic strip due to nonuniform heat supply", *Compos. Struct.* **68**:4 (2005), 471–479.
- [Ramirez et al. 2006] F. Ramirez, P. R. Heyliger, and E. Pan, "Free vibration response of two-dimensional magneto-electro-elastic laminated plates", *J. Sound Vib.* **292** (2006), 626–644.
- [Reddy 1984] J. N. Reddy, *An introduction to the finite element method*, McGraw-Hill, Singapore, 1984. International Editions.
- [Ross 1990] C. T. F. Ross, *Pressure Vessels under External Pressure: Static and Dynamics*, Elsevier Applied Science, London, 1990.
- [Sunar et al. 2002] M. Sunar, Z. Ahmed, M. H. A. Al-Garni, and R. Kahraman, "Finite Element modeling of thermopiezomagnetic smart structures", *AIAA J.* **40** (2002), 1846–1851.
- [Tan and Tong 2002] P. Tan and L. Tong, "Modeling for the electro-magneto-thermo-elastic properties of piezoelectric-magnetic fiber reinforced composites", *Compos. Part A* **33** (2002), 631–645.

- [Tianhu et al. 2002] H. Tianhu, T. Xiaogeng, and S. Yapeng, “Two-dimensional generalized thermal shock problem of a thick piezoelectric plate of infinite extent”, *Int. J. Eng. Sci.* **40** (2002), 2249–2264.
- [Vel and Batra 2000] S. S. Vel and R. C. Batra, “Three-dimensional analytical solution for hybrid multilayered piezoelectric plates”, *J. Appl. Mech.* **67** (2000), 558–567.
- [Wang and Zhong 2003] X. Wang and Z. Zhong, “A finitely long circular cylindrical shell of piezoelectric/piezomagnetic composite under pressuring and temperature change”, *Int. J. Eng. Sci.* **41** (2003), 2429–2445.

Received 16 Sep 2006. Accepted 27 Jan 2007.

N. GANESAN: nganesan@iitm.ac.in

Department of Mechanical Engineering, Indian Institute of Technology, Madras, Chennai 600 036, India

A. KUMARAVEL: ME05D004@iitm.ac.in

Department of Mechanical Engineering, Indian Institute of Technology, Madras, Chennai 600 036, India

RAJU SETHURAMAN: sethu@iitm.ac.in

Department of Mechanical Engineering, Indian Institute of Technology, Madras, Chennai 600 036, India